JOURNAL OF GEOPHYSICAL RESEARCH, VOL. 114, D22101, doi:10.1029/2009JD012405, 2009

Local air-sea interaction in Intertropical Convergence Zone simulations

Anmin Duan,[1] Chung-Hsiung Sui,[2] and Guoxiong Wu[1]

Received 3 May 2009; revised 19 July 2009; accepted 24 August 2009; published 17 November 2009.

[1] We investigate how air-sea interaction affects an Intertropical Convergence Zone (ITCZ) simulation in the SAMIL2.08 atmospheric general circulation model (AGCM). In a control experiment (Exp1) with the observed sea surface temperature (SST) prescribed in the AGCM, there exists a problem of excessive precipitation over much of the Tropics and insufficient precipitation over the equatorial Indian Ocean and the Pacific. The equatorial drought belt arises from the compensatory descending motion associated with exaggerated deep convection over the tropics in both hemispheres. A double ITCZ disappears in a coupled experiment (Exp2) with the same AGCM as used in Exp1 coupled to an interactive ocean mixed layer within the great warm pool. This finding demonstrates that local air-sea interaction can modify the SST pattern, thereby regulating the climate mean state via the following processes. Local air-sea flux exchanges in tropical convective regions such as the ITCZ tend to cool SST via negative cloud-radiation and wind-evaporation feedbacks. Such changes further modify the tropical atmospheric circulation structure such that the equatorial compensatory descent in Exp1 is replaced by the equatorial convergence zone, as seen in nature. A third sensitivity experiment (Exp3), with the AGCM driven by the monthly SST field derived from the coupled experiment, yielded similar results to those obtained in Exp2. Overall, the results indicate that a reasonable depiction of the air-sea coupling process is important to successfully simulating the tropical precipitation pattern, as the atmosphere is closely coupled with the ocean over the tropics.

Citation: Duan, A., C.-H. Sui, and G. Wu (2009), Local air-sea interaction in Intertropical Convergence Zone simulations, *J. Geophys. Res.*, *114*, D22101, doi:10.1029/2009JD012405.

1. Introduction

[2] The Intertropical Convergence Zone (ITCZ) is the region where low-level air converges and rises into the upward branch of the Hadley and Walker circulation. The most identifiable double ITCZ is found over the eastern Pacific during the boreal spring, mainly in March and April. Weak signals of a double ITCZ exist over the Indian Ocean during November, although only infrequently. The signature of a double ITCZ is commonly found over the western and central Pacific, generally between June and September. Over the Atlantic Ocean, however, no double ITCZ is found [*Zhang*, 2001].

[3] In a recent study that made use of surface-wind divergence data obtained from scatterometers on board the ERS-1/2 and QuikSCAT satellites and cloud data obtained from the International Satellite Cloud Climatology Project and Advanced Very High Resolution Radiometer (AVHRR) data, *Meenu et al.* [2007] demonstrated that the double-ITCZ structure is discernible in April, November, and December in the 50°–85°E longitude band over the tropical Indian Ocean. The most probable latitude of occurrence of the double-ITCZ northern band in November and December is ~6°N, and that of the southern band is ~7°S; the equatorial band of surface-wind divergence that separates these two bands is located close to the equator.

[4] Many existing state-of-art atmospheric general circulation models (AGCMs) and coupled atmosphere-ocean global climate models (CGCMs) fail to reproduce the observed tropical rainfall patterns [e.g., *Waliser et al.*, 2003; *Lin*, 2007]. For example, the atmospheric component of the Community Climate System Model (CCSM) Community Atmosphere Model version 3 (CAM3) continues to exhibit a number of long-standing biases, such as a tendency to produce double ITCZ-like structures in the deep Tropics and to overestimate precipitation rates poleward of extratropical storm tracks [*Hack et al.*, 2006].

[5] The double-ITCZ problem in most of the current CGCMs is commonly characterized by insufficient precipitation over the equatorial Pacific and excessive precipitation over the rest of tropics (e.g., Northern Hemisphere ITCZ, South Pacific convergence zone, Maritime Continent, and equatorial Indian Ocean). The excessive precipitation over the extensive tropical oceans usually causes overly

[1] State Key Laboratory of Numerical Modelling for Atmospheric Sciences and Geophysical Fluid Dynamics, Institute of Atmospheric Physics, Chinese Academy of Sciences, Beijing, China.
[2] Graduate Institute of Hydrological and Oceanic Sciences, National Central University, Jhongli, Taiwan.

0148-0227/09/2009JD012405$09.00

strong trade winds, excessive latent heat flux (LHF), and insufficient surface shortwave flux (SWF), leading in turn to a significant cold sea surface temperature (SST) bias over much of the tropical oceans [*Lin*, 2007].

[6] *Dai* [2006] analyzed the precipitation pattern produced by twentieth-century climate simulations using the newest generation of 18 coupled climate system models and compared the results with available observations. The findings of this comparison indicate that although most models reproduce the observed broad patterns of precipitation amount and year-to-year variability, models without flux corrections still show an unrealistic double-ITCZ pattern over the tropical Pacific.

[7] It is widely accepted that ocean-atmosphere feedback plays an important role in determining the tropical mean climate [*Wang*, 2006]. In the great warm pool (GWP; i.e., ocean areas with annual mean SST above 28°C across the Indian Ocean and Western Pacific), local air-sea interaction (i.e., surface heat flux exchange, wind stress from the atmosphere on the ocean, and freshwater flux exchange) dominates the large-scale ocean dynamics [*Webster et al.*, 1998; *Wang*, 2006]. Our recent work indicates that when local air-sea interaction is introduced, the simulated Asia summer monsoon climatology shows a substantial improvement in both the precipitation distribution and timing of the monsoon onset, compared with the AGCM alone [*Duan et al.*, 2008] (herein referred to as DSW2008).

[8] Previous studies have argued that the double-ITCZ problem mainly arises from atmospheric models rather than ocean models [e.g., *Schneider*, 2002]; however, the degree to which air-sea coupling can regulate the tropical precipitation pattern remains to be determined. The motivation behind the present study, therefore, is to investigate the potential impacts of local air-sea interaction in the GWP on the simulation of a double ITCZ in AGCMs.

[9] The remainder of the manuscript is organized as follows. Section 2 describes the data, models, and experimental framework. Section 3 presents the simulation results and considers the factors responsible for discrepancies in simulating the tropical precipitation pattern among experiments with and without air-sea coupling. Finally, Section 4 contains a brief summary of the results and a discussion.

2. Data, Models, and Experiment Design

2.1. Data

[10] We used pentad CPC Merged Analysis of Precipitation data (CMAP) [*Xie and Arkin*, 1997] for the period 1979–1998 to explore the spatial and temporal nature of tropical precipitation. The daily NCEP/DOE reanalysis data set [*Kanamitsu et al.*, 2002] for the same period was employed to diagnose the surface heat balance and the structure of atmospheric circulation. Variables included surface heat flux, surface wind stresses, wind speed in the zonal and meridional directions, and vertical velocity at 17 standard pressures. The horizontal resolution was 1.875° × 1.875° for NCEP/DOE surface variables and 2.5° × 2.5° for variables in the upper layers and CMAP precipitation. Considering the fact that the quality of surface heat flux in nowadays reanalysis data sets is poor, we choose the monthly mean net heat fluxes over the global ocean in the resolution of 1.0° × 1.0° during 1985–2004 achieved in OAFlux data [*Yu and Weller*, 2007] as the substitute of the observations. In comparing the data with simulation results, all variables were first interpolated to the same resolution as that in the AGCM.

2.2. Models

[11] SAMIL2.08 is an AGCM developed by the State Key Laboratory of Numerical Modeling for Atmospheric Sciences and Geophysical Fluid Dynamics (LASG)/Institute of Atmospheric Physics (IAP), Beijing, China. The horizontal direction of SAMIL2.08 is rhomboidally truncated at zonal wave number (R42), approximately equal to a grid of 2.8125° longitude and 1.67° latitude. In the vertical direction, 26 layers are adopted in hybrid coordinates. The dynamical framework uses a 'standard atmosphere reduction' scheme [*Zeng*, 1963; *Phillips*, 1973], and a semi-implicit time integration program is introduced. The model includes smoothed topography, gravity wave drag, and predicted clouds. The radiation scheme is from *Edwards and Slingo* [1996]. Processes of convection and condensation are parameterized using a mass-flux scheme [*Tiedtke*, 1989], and the SSiB model [*Xue et al.*, 1991; *Liu and Wu*, 1997] is implemented for land-surface processes. A more detailed description of the model, including an account of recent improvements, is given by *Zhou et al.* [2005].

[12] The ocean mixed layer model (OMLM) used in this work is a second-order turbulence closure model [*Noh and Kim*, 1999; *Noh et al.*, 2002]. A number of important aspects of this OMLM have been improved over earlier models, including the surface boundary conditions for turbulent kinetic energy, the parameterization of stratification effects on turbulence, and the design of convective processes. The model can successfully simulate the temporal evolution of profiles of dissipation rate and temperature, and reproduces various important features of the oceanic boundary layer. This OMLM has previously been coupled to an oceanic general circulation model [*Noh et al.*, 2002] and a CGCM [*Yim et al.*, 2008] in studying many aspects of climate variability.

[13] The model has 50 vertical levels with a uniform thickness of 5 m. Based on the results of a sensitivity experiment, the important empirical parameter α, which determines the dependence of the mixing length on stratification, is set to 5. Considering that the turbulent kinetic energy in the GWP is particularly large after onset of the monsoon, the empirical constant m, which determines the turbulent kinetic energy flux at the sea surface, is set to 400. As in DSW2008, the restoring time scale of SST is chosen as 5 days.

2.3. Experiment Description

[14] The basic experiment design is similar to that employed in DSW2008, with three experiments being performed. Exp1 is the AGCM control run, in which the 20 year averaged monthly SST and sea ice data, as required by the Atmospheric Model Intercomparison Project (AMIP) II (for details, see http://www-pcmdi.llnl.gov/projects/amip/AMIP2EXPDSN/BCS_OBS/amip2_bcs.htm), are prescribed and interpolated linearly to each integration step. These procedures exclude the impacts of interannual ocean variability (e.g., El Niño). The results of this experiment are then used to examine the general performance of the AGCM.

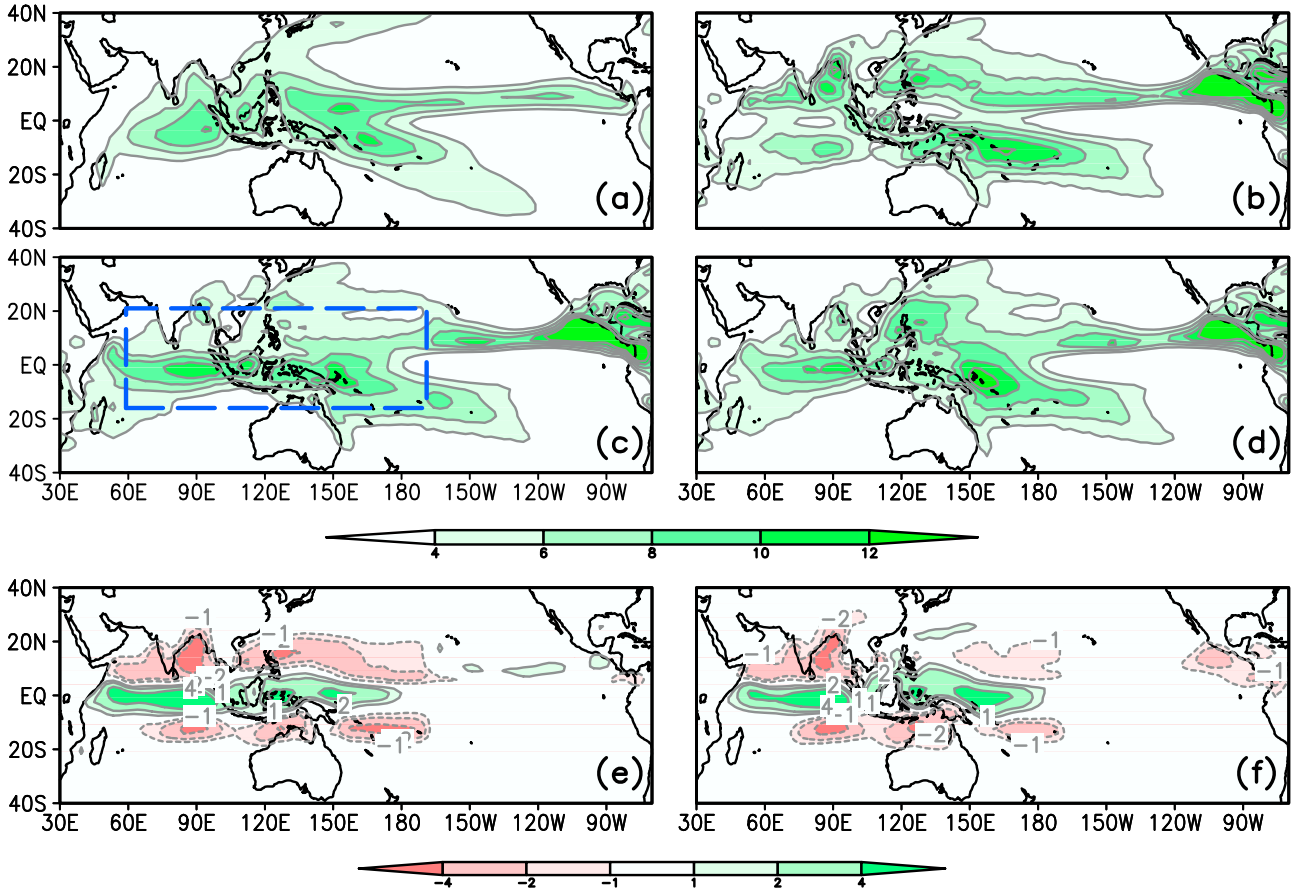

Figure 1. Annual mean precipitation fields in (a) CMAP, (b) Exp1, (c) Exp2, and (d) Exp3. Also shown are the difference fields for (e) Exp2 minus Exp1 and (f) Exp3 minus Exp1. Unit is mm day^{-1}. The dashed rectangle in Figure 1c represents the coupling area in the GWP.

[15] Exp2 is a coupled AGCM-OMLM run in which the *Noh and Kim* [1999] OMLM is coupled to SAMIL2.08 in a rectangle box including most parts of the GWP (15.76°S–20.737°N; 59.0625°E–191.25°E). For the remaining ocean grids, SST is the same as that in Exp1. Note that in addition to the net surface heat flux and wind stresses, here the freshwater flux is introduced in the air-sea coupled area at each integration step (600 s). In this way, the short-range signals in SST, including the diurnal cycle, are accommodated in the coupled system. Discontinuity of SST at the boundary between the coupled region and outside will generate spurious wind field to a certain degree. However, due to the relatively coarse horizontal resolution in SAMIL, this problem is not serious.

[16] Exp3 is an AGCM sensitivity run, similar to Exp1 except that the SST forcing field is caused by Exp2 instead of observation data. The purpose of this experiment is to consider the influence of SST alone upon the AGCM with a mean state similar to that in Exp2.

[17] Each of the three experiments was integrated for 22 years, and the output of the last 20 years was averaged to enable a comparison with the 20 year mean (1979–1998) in NCEP/DOE or CMAP. The difference between Exp1 and Exp2 represents the combined contribution of the modified SST field and air-sea feedback. Since the monthly SST is employed as the forcing field in Exp3, the difference between Exp2 and Exp3 accounts for the SST effect on submonthly timescale, as suggested by *Fu and Wang* [2004].

3. Results

3.1. Precipitation and SST

[18] Figure 1 shows the spatial distribution of annul mean tropical precipitation, as determined from observations and the three experiments. The observed precipitation features in CMAP (Figure 1a) include a broad precipitation zone over the tropical Indian and two ITCZs (represented by the 6 mm day^{-1} contour) in the Pacific. The Northern Hemisphere ITCZ is located at 5°–10°N and spans the entire tropical Pacific, whereas the southern Pacific ITCZ, at 5°–10°S, extends only to 150°W. These two branches merge in the equatorial Western Pacific. Two precipitation maxima (above 10 mm day^{-1}) are seen off the equatorial Western Pacific (i.e., near 155°E, 5°N and 165°E, 5°S). Two other relatively weak centers (rainfall above 8 mm day^{-1}) appear in the equatorial Eastern Indian Ocean and Maritime Continent, with the main part of the former occurring slightly southward of the equator. We then compare the simulated precipitation distribution in Exp1–3 against the observed climatology.

[19] In Exp1 (Figure 1b), the equatorial zone from the Eastern Indian Ocean to the Western Pacific becomes too dry (annual mean precipitation of 6 mm day^{-1}). In contrast,

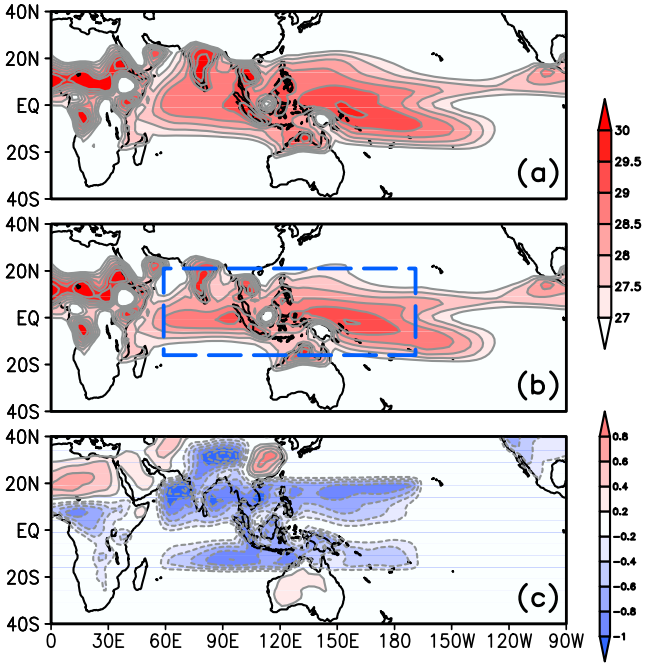

Figure 2. Annual mean SST and land-surface temperature values in (a) Exp1 and (b) Exp2, as well as (c) their difference (Exp2 minus Exp1). Unit is °C. The dashed rectangle in Figure 2b represents the coupling area in the GWP.

abnormally strong precipitation occurs in neighboring Tropics including the Indian monsoon region, Bay of Bengal, Philippine Sea, south Indian Ocean, and the South Pacific convergence zone (SPCZ) within the Southern Hemisphere. This pattern is the characteristic feature of the so-called double-ITCZ problem in current AGCMs and CGCMs.

[20] When local air-sea interaction is introduced in Exp2, the overly strong double ITCZ found in Exp1 disappears; consequently, the simulated large-scale precipitation pattern (Figure 1c) seems to be more consistent with observations. In other words, overestimated (underestimated) precipitation over the Tropics (near the equator) has been substantially mitigated. Outside the GWP, where air-sea coupling processes are not allowed, the precipitation pattern resembles that in Exp1.

[21] The simulated precipitation in Exp3 (Figure 1d) shows a similar pattern to that in Exp2, except that the magnitude over the South China Sea and Philippine Sea is somewhat stronger (about 2–4 mm day^{-1} more). Details in precipitation difference among the three experiments are shown in Figures 1e and 1f, in which we observe an equatorward displacement of the chief precipitation belt from Exp1 to Exp2 and Exp3. This result highlights the fact that equatorial precipitation is closely connected to precipitation north and south of the equator.

[22] In the coupled experiment Exp2, SST is the only variable returned directly from the ocean to the atmosphere; therefore, all of the differences in the atmosphere between Exp1 and Exp2 can be attributed to differences in the atmospheric lower boundary condition and the inherent processes of air-sea interaction. Figure 2 shows the spatial distribution of annual mean SST and land-surface temperature in Exp1 and Exp2, and the difference between the two sets of values. Of note, the SST field in Exp1 is the climatology indicated by observations, and SST in Exp3 is the same as that in Exp2.

[23] In comparing Figures 2a and 2b with Figures 1a–1d, we immediately observe a similar spatial distribution between areas of warm SST and areas of high precipitation, suggesting that the SST field is the primary factor in generating the basic pattern of tropical precipitation. As documented in many previous studies, warm SST provides a suitable background for convection development via increased lower atmospheric instability and moisture convergence [e.g., *Wu*, 2002; *Duan et al.*, 2008]. The SST difference field between Exp1 and Exp2 (Figure 2c) demonstrates that local air-sea interaction tends to cool the SST across most parts of the GWP, especially near the west coast of the Indian Peninsula, Bay of Bengal, South China Sea, Philippine Sea, and the southern tropical Indian Ocean, in which areas the amplitude exceeds −0.8°C. The SST difference is negligible near the equator (within ±0.2°C). It is clear that the equatorial precipitation difference between Exp1 and Exp2 is induced mainly by large-scale circulation shift rather than local SST change.

3.2. Air-Sea Feedback Responsible for SST Change

[24] Generally speaking, there are three types of air-sea feedback in the tropical mean climate system (for a summary, see *Lin* [2007]). The first is a positive feedback between SST gradient and the trade winds, known as Bjerknes feedback. We believe that this feedback is unlikely to be important in Exp2 because (i) air-sea coupling is only allowed in the GWP domain and the cold tongue in the eastern Pacific is equivalent to observations, and (ii) the simulated SST shows a clear meridional gradient rather than a zonal gradient.

[25] The second air-sea feedback is that between SST and surface LHF [e.g., *Wallace*, 1992]. In this mechanism, a perturbation in SST affects the surface wind speed, surface air humidity, and sea-air humidity difference, leading to changes in the surface LHF, which in turn modifies SST. The sign of SST-LHF feedback varies over space and time [e.g., *Liu et al.*, 1994; *Zhang and McFarlane*, 1995], although it is generally negative in the GWP [e.g., *Wu*, 2002].

[26] Finally, the third air sea feedback is that between SST and SWF [e.g., *Ramanathan and Collins*, 1991; *Peters and Bretherton*, 2005]. Previous studies have indicated that this feedback is negative in the warm pool [e.g., *Klein and Hartmann*, 1993; *Wu*, 2002]. In this case, high SST leads to an increase in the activity of deep convection and more clouds, which in turn reduces the surface downward SWF into the ocean, thereby cooling SST. The effect of wind stress in modulating SST is also expected to be important, as strong wind stress can stir the ocean more efficiently and deepen the ocean mixed layer, resulting in reduced SST. The influence of fresh water flux on stratification of the ocean mixed layer (and hence SST variation) is also included in Exp2. The existence of a cold SST bias in Exp2 compared with Exp1 indicates that negative SST LHF and/or SST SWF feedbacks, together with the effect of wind stress, are likely to play a dominant role in air sea coupling processes in the GWP. In fact, further examine the difference in SWF and LHF between Exp1 and Exp2, we could find that the SST

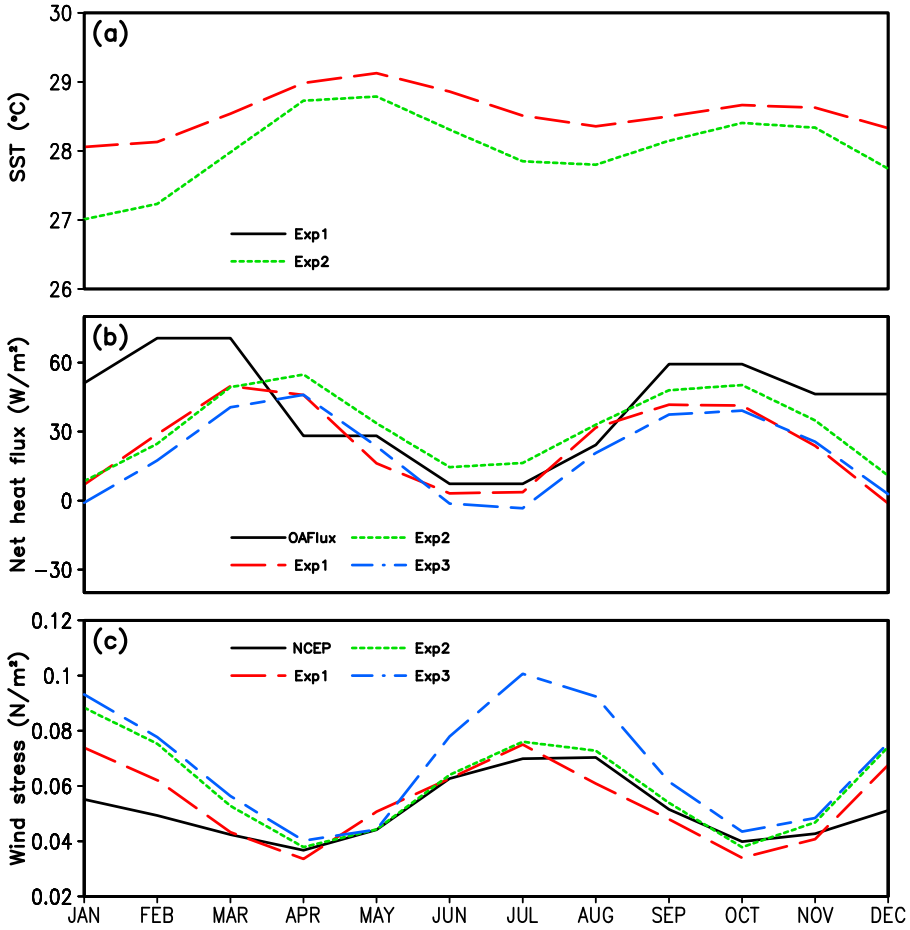

Figure 3. Annual cycles in (a) SST, (b) net surface heat flux, and (c) surface wind stress over the GWP.

LHF feedback is more important than the SST SWF feedback for the domain averaged case (figures not shown here).

[27] In Figure 3, we present the GWP domain averaged annual cycle of SST, net surface heat flux, and wind stress in observation and the three experiments. Air sea coupling not only acts to cool SST in the GWP, but magnifies the amplitude of its annual cycle. The amplitude of the SST annual cycle is 1.2°C in Exp1 and 2°C in Exp2 (Figure 3a). Figure 3b shows the annual cycle of the GWP domain averaged net surface heat flux. In each experiment, the model generated net surface heat flux presents a much less magnitude (around 40 W m^{-2}) than that in OAFlux during the boreal winter half year while the difference in the summer is small (within ±10 W m^{-2}). Figure 3c shows the annual cycle in surface wind stress, which is proportional to the square root of zonal and meridional winds. During the boreal winter (December–February), all three experiments tend to generate a strong wind stress, whereas the wind stresses in Exp1 and Exp2 during the other months of the year are comparable to that in NCEP/DOE. The wind stress in Exp3 is clearly overestimated in June, July, and August. Thereby, weaker incoming heat flux and stronger wind stress during the boreal winter are consistent with the cold bias in Exp2. Intercomparison among those three experiments suggests that the intrinsic disadvantages in the AGCM have been inherited in the coupled model and it should be responsible primarily for the larger amplitude in SST annual cycle in Exp2. Moreover, the larger wind stress bias produced by Exp3 implies that air sea feedback in the coupled model efficiently regulates the wind stress via changing the atmospheric lower boundary condition, particularly during the boreal summer. Detailed physical mechanisms have been documented by *Wallace* [1992].

[28] To enable a more quantitative evaluation of SST biases, Figure 4 shows zonal profiles of annual mean SST along the Tropics and the equator region. In addition to a seasonal dependence, the biases in SST show a clear meridional structure. The air sea coupled run (Exp2) produces a cold SST bias (−1°C at most) away from the equator in both hemispheres. Along the equator, the cold bias is relatively small (less than −0.2°C), except over land areas such as Sumatra (∼100°E), Kalimantan (∼115°E), and West Sura Prestige island of Indonesia (∼120°E).

[29] Figure 5 is same as Figure 4, but for precipitation. Compared with CMAP, Exp2, and Exp3, Exp1 simulates excessive precipitation over much of the Tropics and insufficient precipitation along the equator, except in the Maritime Continent where the precipitation bias is relative small. In the Indian Ocean sector, large biases occur in the northern tropical belt (about +4 mm day^{-1}) and the equatorial belt (about −4 mm day^{-1}). In the Western Pacific sector, however, the largest precipitation bias in Exp1 is found in the southern tropical belt (roughly +4 mm day^{-1}) and along the equator (near −3 mm day^{-1}). The small SST

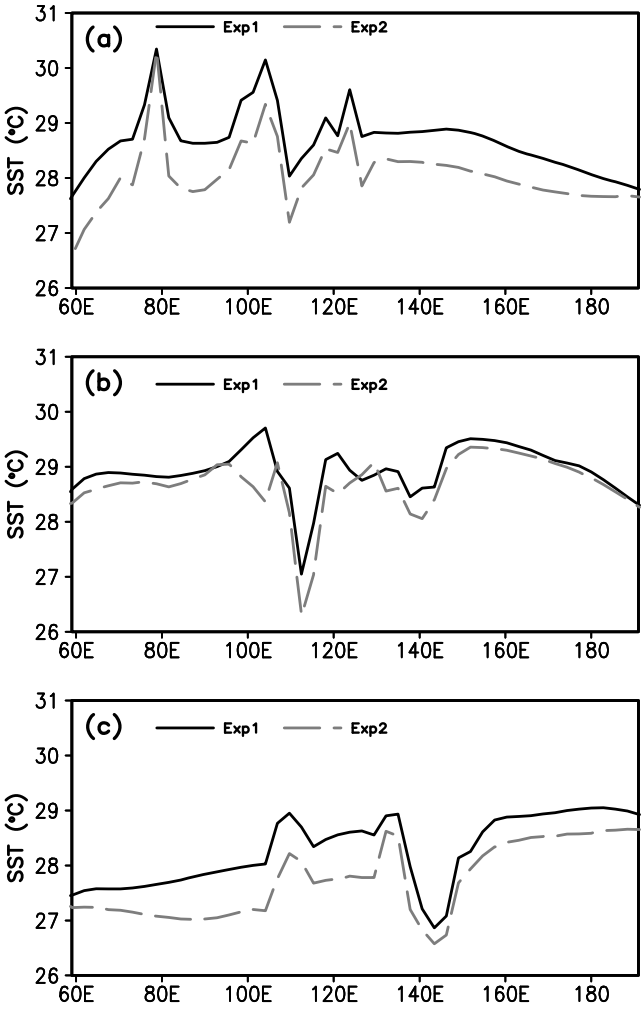

Figure 4. Annual mean SST averaged over the regions (a) 5°N–15°N, (b) 5°S–5°N, and (c) 5°S–15°S.

bias along the equator but large difference in the precipitation bias between Exp1 and Exp2 indicates that deep convection in the AGCM is not controlled solely by local SST, it is also influenced by other processes such as large scale atmospheric circulation and the SST gradient [e.g., *Lindzen and Nigam*, 1987].

[30] The double ITCZ problem also manifests itself in the latitudinal asymmetry of SST and precipitation. Figure 6 shows the interhemispheric differences (average over 5°–15°N minus the average over 5°–15°S) for annual mean SST (Figure 6a) and precipitation (Figure 6b). Exp2 produces a satisfactory latitudinal SST asymmetry over the GWP and generates a larger asymmetry in precipitation, as in nature. A similar situation can be seen in Exp3. Exp1 produces a weak asymmetry in latitudinal precipitation over the GWP. The precipitation differences among these experiments suggest that the observed SST prescribed in Exp1 simply cannot reproduce the corresponding rainfall pattern as observed in the current model. This may reflect a model bias as a result of imperfect physical schemes in the current model. This may also indicate the effect of local air sea interaction in maintaining observed SST which is lacking in Exp1. Namely, in nature, after the onset of Asian summer monsoon, negative SST LHF and SST SWF feedbacks, together with the deepened ocean mixed layer induced by the enhanced surface wind stress, cools down the beneath SST efficiently. The above SST change, however, is absent in Exp1. Instead, SST is prescribed as the lower boundary forcing condition. Persistent high SST will provide more moisture convergence and more unstable lower atmosphere and hence the largely overestimated summer monsoon precipitation. Therefore, in addition to the use of incomplete physical schemes, the absence of air sea feedback is the other likely reason for the occurrence of the double ITCZ problem. In fact, the importance of the ocean model component in simulating the ITCZ has been reported in previous studies. For example, in comparing the CGCMs of GISS ER and GISS EH, which have identical atmospheric models but different ocean models, *Lin* [2007] found that they produce dramatically different mean climate, with a double ITCZ problem in GISS EH but not in GISS ER.

[31] Now that we have identified the double ITCZ problem and its dependence on air sea interaction, we need to further clarify what types of air sea feedback are responsible for the SST change. Figure 7 shows the annual mean wind stresses in the zonal and meridional directions along different latitudinal belts. Geographical variations in the three experiments are similar to those in NCEP/DOE reanalysis.

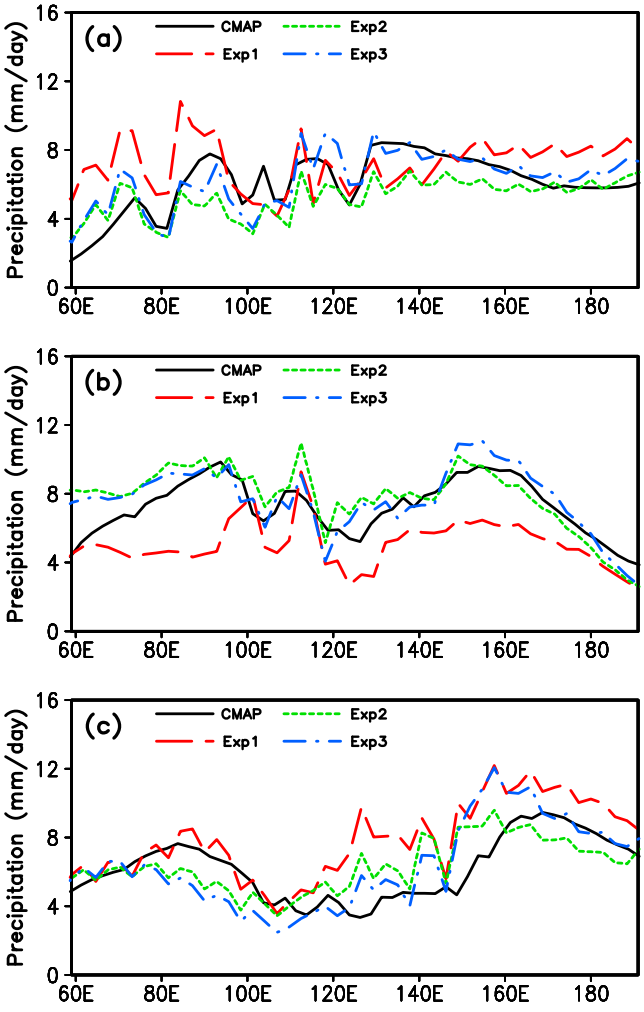

Figure 5. As in Figure 4 but for precipitation.

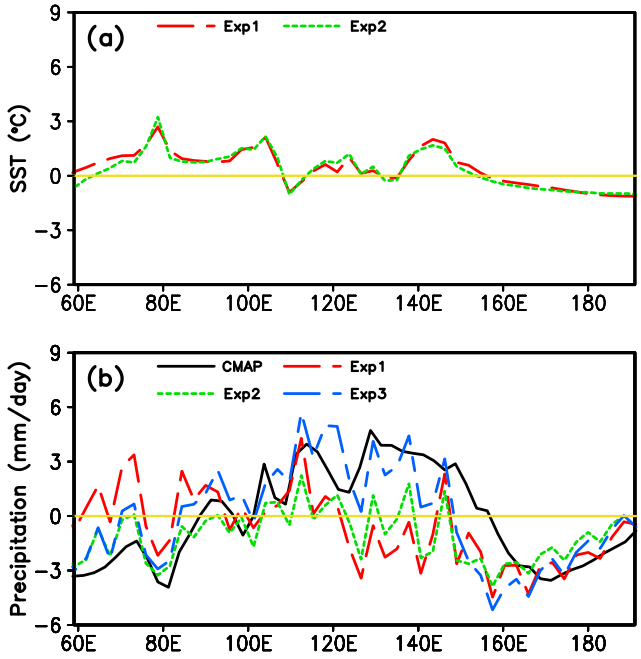

Figure 6. Interhemispheric differences (average over 5°N–15°N minus the average over 15°S–5°S) in annual mean (a) SST and (b) precipitation.

In tropical oceans, the zonal wind stress dominates its meridional counterpart (note the different scales used in Figures 7a, 7c, and 7e versus Figures 7b, 7d, and 7f). Within the GWP basin, a westward annual mean wind stress (negative zonal wind stress) is only seen in the eastern part of the Northern Indian Ocean, and wind stresses are generally weak near the equator. Over the southern Tropics, the zonal and meridional wind stresses produced by Exp2 and Exp3 are similar to those in NCEP/DOE reanalysis, whereas Exp1 tends to generate much weaker wind stresses.

[32] Strong wind stress acts to stir the underneath ocean more efficiently, deepen the ocean mixed layer, and cool the in situ SST. Over the northern Tropics, however, the situation appears more complicated. In the South China Sea and Western Pacific (105°–170°E), wind stresses in Exp2 and Exp3 (Exp1) are stronger (weaker) than those in NCEP/DOE reanalysis. For the Indian Ocean (60°–100°E), wind stresses in Exp2 and Exp3 are weaker than those in Exp1, indicating that the stirring effect of wind stress seems to be less pronounced in this region.

[33] Besides directly forcing the ocean mixed layer, the surface wind biases lead to biases in LHF (Figures 8a, 8c, and 8e). Positive values of LHF indicate that the ocean loses heat and transfers vapor to the atmosphere above. The models always generate larger LHF than that observed, not only

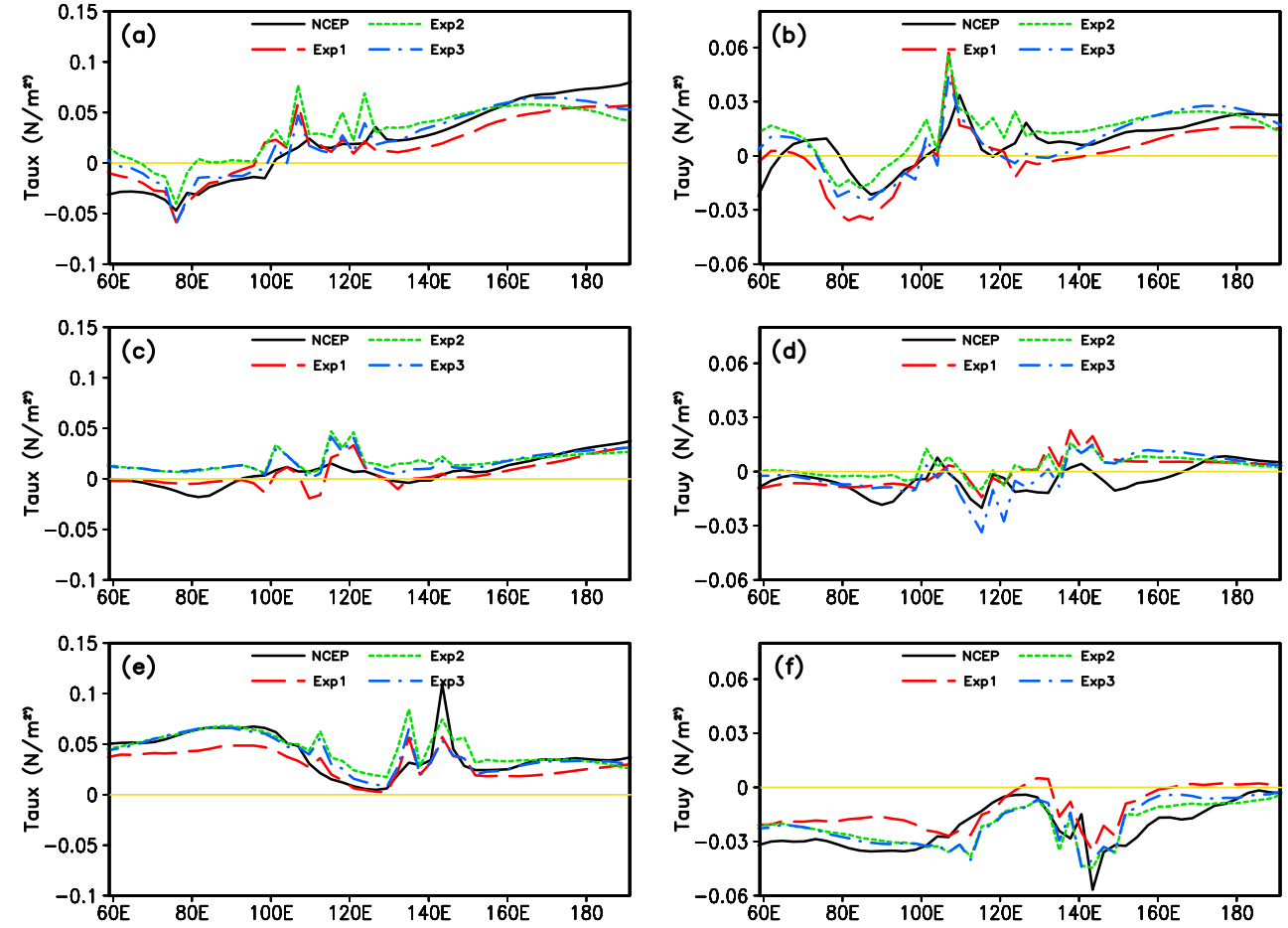

Figure 7. (a, c, and e) Annual mean eastward surface wind stress, τ_x, (b, d, and f) annual mean northward surface wind stress, τ_y, averaged over the regions 5°N–15°N (Figures 7a and 7b), 5°S–5°N (Figures 7c and 7d), and 5°S–15°S (Figures 7e and 7f).

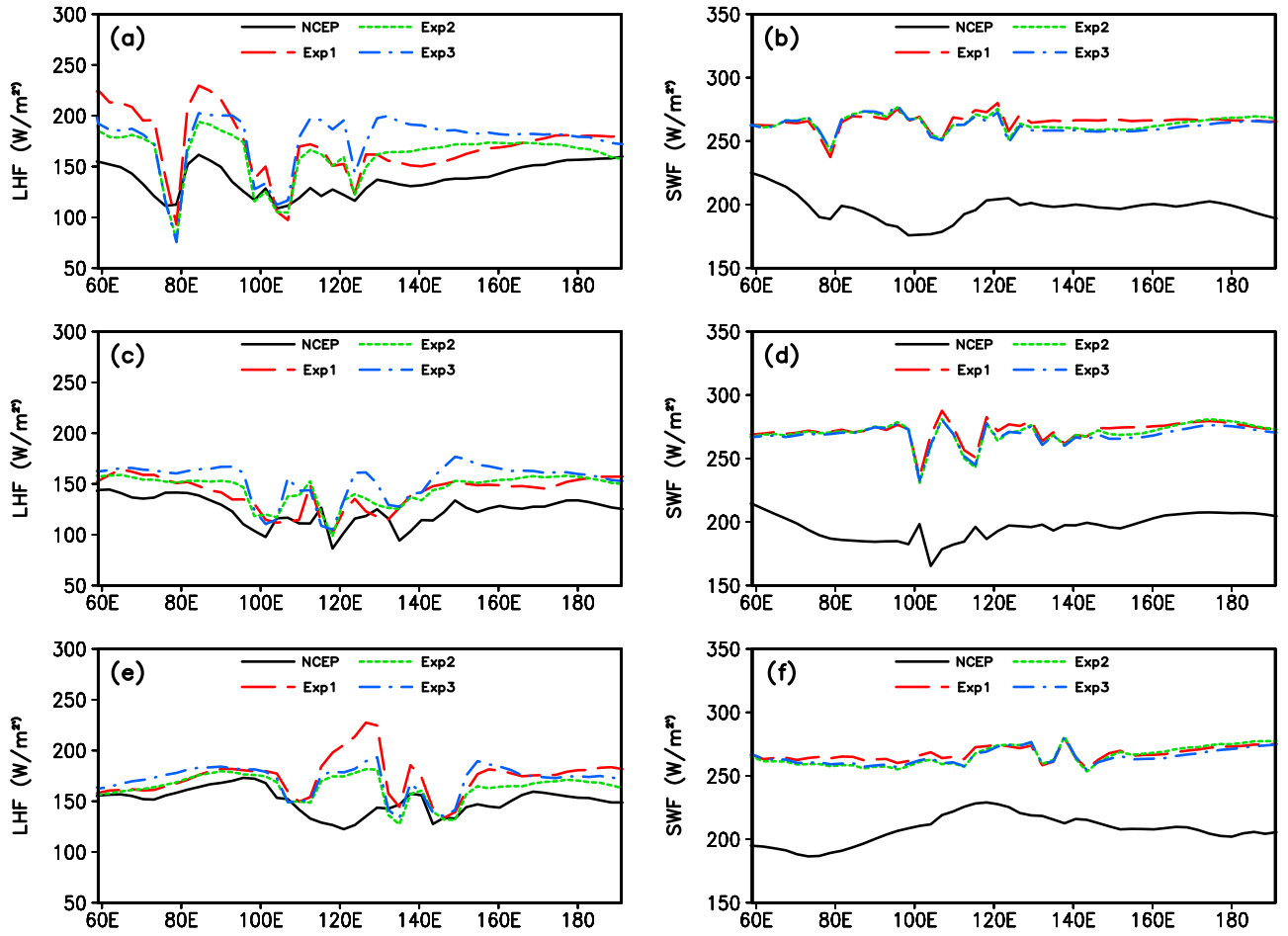

Figure 8. (a, c, and e) Annual mean upward LHF and (b, d, and f) annual mean downward SWF averaged over the regions 5°N–15°N (Figures 8a and 8b), 5°S–5°N (Figures 8c and 8d), and 5°S–15°S (Figures 8e and 8f).

in the AGCM runs but also in the coupled run. This discrepancy is associated with the larger rainfall amount over warm oceans. In some areas (e.g., the north Indian Ocean and SPCZ), the situation is clearly improved in Exp2. Excessive LHF contributes to a cold SST bias in Exp2 over much of the tropical oceans via negative SST LHF feedback.

[34] In addition to LHF, SWF is a dominant term of the net surface flux. All three experiments yield a systematic error in SWF of nearly 50 W m^{-2}. This error is apparently derived from an intrinsic defect in the AGCM, probably the small amount of stratus cloud in the model (figure not shown).

[35] As with SST and precipitation, a clear meridional asymmetry is observed in the spatial structure of the difference fields in surface net heat flux and wind stress among the three experiments (Figure 9). Significant differences in heat flux and wind stress occur in the Tropics rather than along the equator. In general a cold SST bias agrees with reduced downward net heat flux and enhanced wind stress. An exceptional case is found in the north Indian Ocean, where Exp2 and Exp3 produce reduced net heat flux but weaker wind stress. However, between 20°S and the Equator to the northwest Australia, stronger surface wind stress in Exp2 than Exp1 and the resultant more efficient vertical mixing in the upper ocean should be the main factor for the cold SST difference in Exp2. In the local air sea coupled model, it is clear that the mechanisms responsible for the SST cold bias across the GWP vary spatially and seasonally. In comparing Exp2 with Exp1, and comparing Exp3 with Exp1, the surface net heat flux and wind stress have the same sign but a small difference. This indicates that air sea interaction provides an AGCM with a more physically consistent response to oceanic forcing.

3.3. Response of Atmospheric Circulation to Air-Sea Interaction

[36] Here we consider why the coupled experiment with a cold SST bias was successful in alleviating the double ITCZ problem. Atmospheric circulation over the Tropics and equator are closely connected to each other via meridional circulation. During the boreal summer, the Asian monsoon cell is characterized by an intense tropical ascending motion over the Indian Ocean, Bay of Bengal, and South China Sea, as well as a compensatory downward motion over the equatorial region. A similar situation occurs in the Southern Hemisphere during summer. In terms of the annual mean, the strongest ascending motion appears above the equatorial region, between 10°S and 10°N (Figure 10a). In Exp1 (Figure 10b), however, accompanying the double ITCZ,

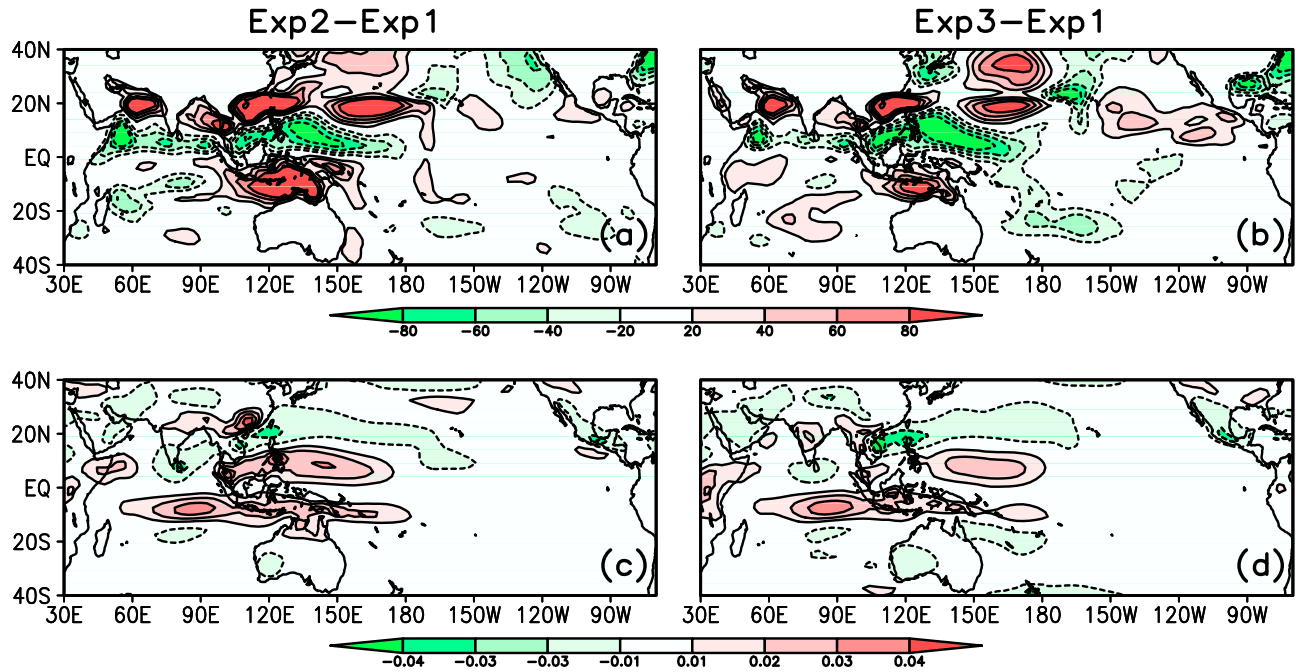

Figure 9. Difference fields in annual mean net (a and b) surface heat flux and (c and d) surface wind stress.

perennial excessive precipitation over the Tropics leads to an equatorial subsidence belt, as required by the conservation of air mass, which in turn limits the development of equatorial convection and the subsequent dry belt. In Exp2, negative SST LHF and SST SWF feedbacks, together with the stirring effect of wind stress act to cool the SST in the double ITCZ, thereby preventing the development of strong convection in the overlying atmosphere. As a result, the

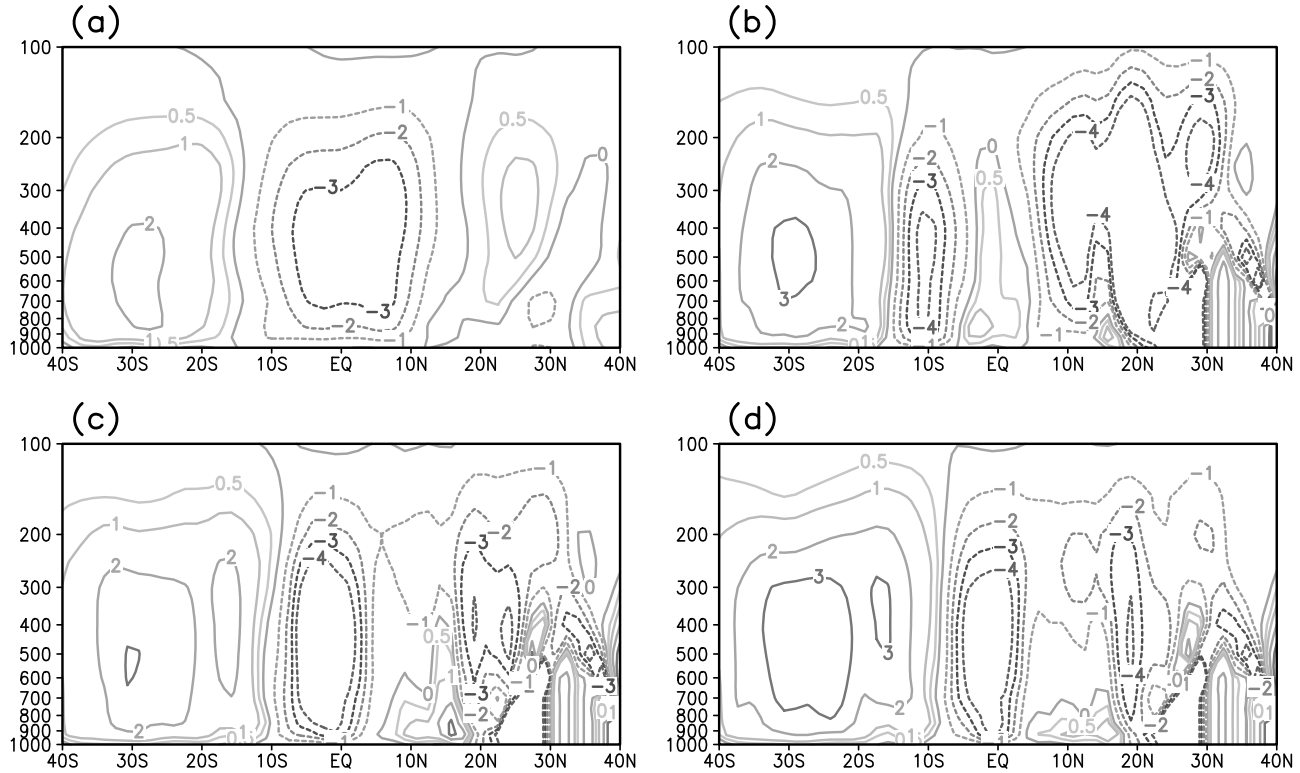

Figure 10. Annual mean meridional cross section of vertical motion, ω, in (a) NCEP/DOE, (b) Exp1, (c) Exp2, and (d) Exp3 averaged for 59°E–191°E. Unit is 100 × Pa s^{-1}. Negative and positive values represent upward and downward motion, respectively.

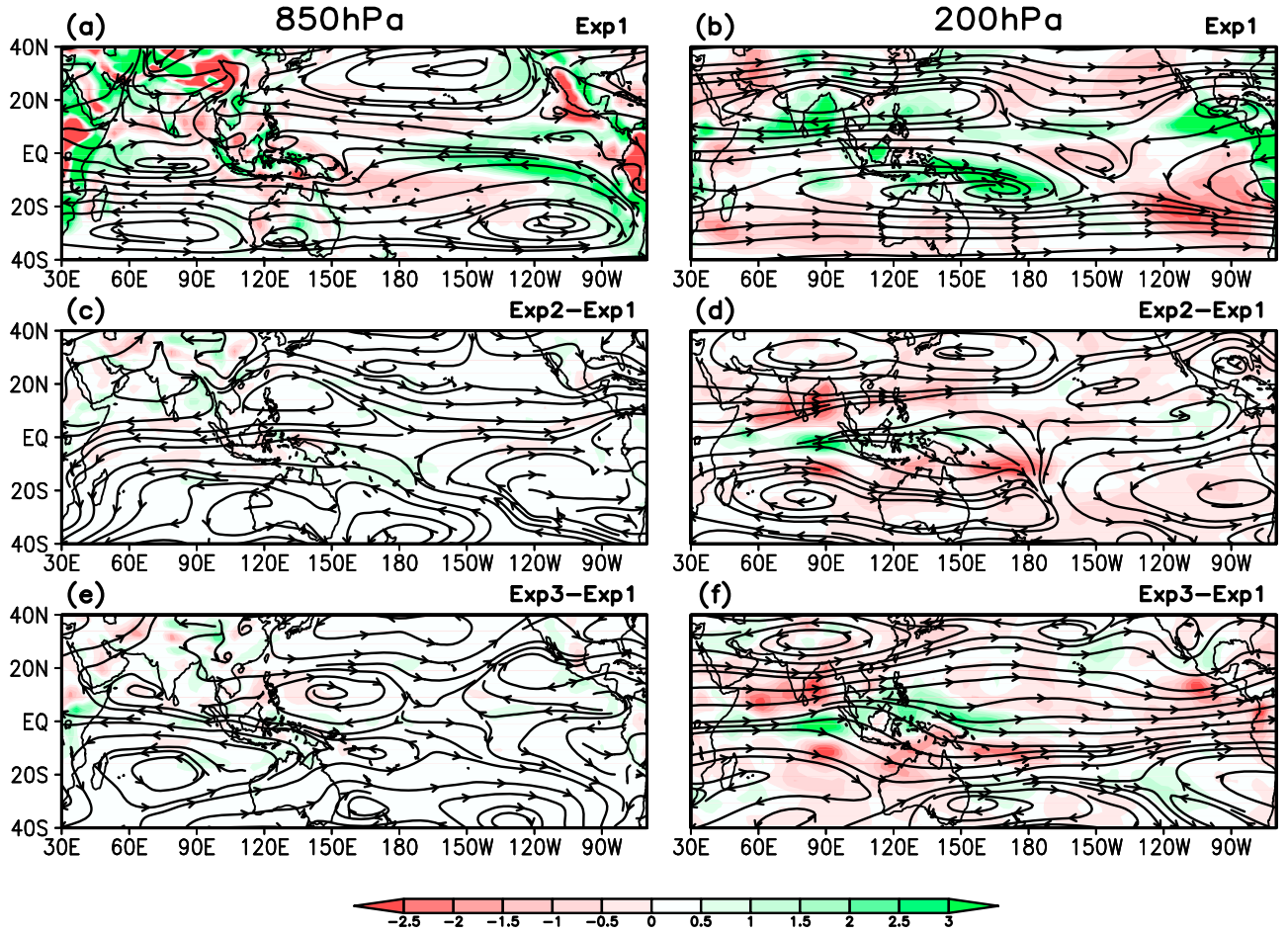

Figure 11. (a and b) Annual mean streamline and divergence fields in Exp1 and the difference fields between (c and d) Exp2 and Exp1 as well as (e and f) Exp3 and Exp1. Units of divergence are $s^{-1} \times 10^6$.

subsidence belt is replaced by a center of ascending motion over the equator; the lateral areas of descending motion act to weaken convection over the northern and southern Tropics (Figure 10c). A similar situation is evident in Exp3 when using the same lower boundary condition (Figure 10d).

[37] As with the vertical velocity field, differences in general circulation among the three experiments are immediately apparent. Figure 11 shows the annual mean streamline and divergence fields in the lower layer (850 hPa) and upper layer (200 hPa), together with the difference fields between Exp2 and Exp1 as well as between Exp3 and Exp1. Compared with Exp1, an anomalous tropical easterly at 850 hPa appears over the Indian Ocean and the Western Pacific in Exp2 and Exp3. For the Northern Tropics and the near-equator region, this wind blows against the climatological wind direction, thereby reducing the intensity of the southwesterly jet. Over the south Indian Ocean, however, the anomalous wind direction is consistent with the climatology, reinforcing the easterly current.

[38] Two anomalous tropical anticyclone pairs, located symmetrically about the equator, are observed at 850 hPa. The anticyclones in the Indian Ocean are centered at about 80°E, 20°N and 85°E, 20°S, and those in the Western Pacific are centered at approximately 135°E, 15°N and 130°E, 25°S. Above them, two anomalous cyclone pairs exist in the upper layers, with a clear poleward titling. The configuration of the anomalous atmospheric circulation in Exp2 and Exp3 is featured by the two pairs of anti-Gill-type mode [*Gill*, 1980], which developed in response to the colder SST within the GWP, and have a clearer structure in Exp3 than in Exp2. As a result, divergence in lower layers and convergence in upper layers act to weaken tropical convection in Exp2 and Exp3. Along the equator, a revised vertical structure characterized by convergence in lower layers and divergence in upper layers is indicative of enhanced ascending motion. Therefore, air-sea coupling first modifies the local SST, and then modulates the large-scale pattern of atmospheric circulation and vertical motion structure. Finally, the precipitation pattern adapted to the circulation adjustment in the coupled model represents a reasonable picture of the ITCZ.

4. Summary and Discussion

[39] This study investigates the effect of local air-sea interaction in the tropical warm pool on an AGCM response to the lower boundary forcing. SAMIL2.08 is adopted for the study and a control experiment is carried out to simulate the model response to prescribed climatological SST. In the annual mean sense, the model produces insufficient equatorial precipitation but excessive precipitation in the rest of the tropical Indian Ocean and Western Pacific. The precip-

itation and associated circulation represents a spurious double-ITCZ that appears as a common problem in many GCMS. In another experiment with the same AGCM but coupled to an OMLM in the GWP, the double-ITCZ problem is substantially mitigated. A third experiment with a prescribed forcing field derived from the coupled run exhibits a similar improvement. After diagnosing SST, wind stresses, and heat flux fields in the three experiments, we conclude that local air-sea interaction modulates SST in the GWP through the negative SST-LHF feedback, negative SST-SWF feedback, and the stirring effect of wind stress; however, the relative importance of these three mechanisms varies both spatially and seasonally.

[40] Compared with observations, the coupled run induces two clear off-equator belts of cold SST (by up to $-1.2°C$), roughly within 5°–15°S and 5°–20°N, whereas the SST along the equator region (5°S–5°N) shows only a small bias (within $-0.2°C$). Such a change in the atmospheric lower boundary condition suppresses the development of strong convection over the original double-ITCZ. Consequently, the equatorial compensatory descending belt (as required by mass conservation) in the AGCM control run is replaced by an intense ascending flow and the equatorial maximal precipitation belt, as seen in nature.

[41] Why is the AGCM driven by observed SST unable to produce the real large-scale rainfall pattern over the warm tropical oceans? This may be related to intrinsic defects in the physical parameterization schemes employed by the AGCM. It is also likely due to the absence of air-sea interaction that plays an important role in maintaining SST in the GWP. Therefore, improving the physical schemes would help to mitigate the model bias. Nevertheless, the current study suggest that including the local air-sea feedbacks have a profound influence on the SST field, and hence the mean pattern of the tropical climate.

[42] Although large-scale oceanic advection has been shown to play a secondary role in modifying SST within most parts of the GWP [e.g., *Fu et al.*, 2003], a full consideration of all oceanic factors is required to increase our knowledge of air-sea interaction; however, this in turn requires a high-quality CGCM. In fact, some of current CGCMs produce warmer SST in the GWP domain than that observed [*Dai*, 2006], whereas this work has demonstrated that the main air-sea feedbacks favor a colder SST in the GWP. This unreasonable result obtained from CGCMs serves as a reminder of the difficulties involved in improving numerical depictions of the physical processes that occur in the ocean mixed layer. Our future work will examine changes in the ocean mixed layer over various time scales in our coupled AGCM-OMLM model, as SST not only represents a boundary forcing for the atmosphere; it is also a result of atmospheric variations. Investigations of responses in the underlying ocean mixed layer to the passing of different convective phases will help us to understand the air-sea coupled system in a wider sense.

[43] **Acknowledgments.** We would like to thank Xiuhua Fu and Xuehong Zhang for their valuable suggestions. Duan and Wu were jointly supported by the Chinese Ministry of Science and Technology under grant 2006CB403607 and the R&D Special Fund for Public Welfare Industry (meteorology) administered by the Chinese Ministry of Finance and Ministry of Science and Technology (GYHY200806007). Sui was supported by NSC 95-2111-M-008-003.

References

Dai, A. (2006), Precipitation characteristics in eighteen coupled climate models, *J. Clim.*, *19*, 4605–4630, doi:10.1175/JCLI3884.1.

Duan, A. M., C. S. Sui, and G. X. Wang (2008), Simulation of local air-sea interaction in the great warm pool and its influence on Asian monsoon, *J. Geophys. Res.*, *113*, D22105, doi:10.1029/2008JD010520.

Edwards, J. M., and A. A. Slingo (1996), Studies with a flexible new radiation code. I: Choosing a configuration for a large-scale model, *Q. J. R. Meteorol. Soc.*, *122*, 689–720, doi:10.1002/qj.49712253107.

Fu, X., and B. Wang (2004), Differences of boreal summer intraseasonal oscillations simulated in an atmosphere-ocean coupled model and an atmosphere-only model, *J. Clim.*, *17*, 1263–1271, doi:10.1175/1520-0442(2004)017<1263:DOBSIO>2.0.CO;2.

Fu, X., B. Wang, T. Li, and J. P. McCreary (2003), Coupling between northward propagating intraseasonal oscillations and sea-surface temperature in the Indian Ocean, *J. Atmos. Sci.*, *60*, 1733–1753, doi:10.1175/1520-0469(2003)060<1733:CBNIOA>2.0.CO;2.

Gill, A. E. (1980), Some simple solutions for heat-induced tropical circulation, *Q. J. R. Meteorol. Soc.*, *106*, 447–462, doi:10.1002/qj.49710644905.

Hack, J. J., J. M. Caron, S. G. Yeager, K. W. Oleson, M. M. Holland, J. E. Truesdale, and P. J. Rasch (2006), Simulation of the global hydrological cycle in the CCSM Community Atmosphere Model Version 3(CAM3), mean features, *J. Clim.*, *19*, 2199–2221, doi:10.1175/JCLI3755.1.

Kanamitsu, M., et al. (2002), NCEP-DEO AMIP-II Reanalysis (R-2), *Bull. Am. Meteorol. Soc.*, *83*, 1631–1643, doi:10.1175/BAMS-83-11-1631(2002)083<1631:NAR>2.3.CO;2.

Klein, S. A., and D. L. Hartmann (1993), The seasonal cycle of low stratiform clouds, *J. Clim.*, *6*, 1587–1606.

Lin, J. L. (2007), The double-ITCZ problem in IPCC AR4 coupled GCMs: Ocean-atmosphere feedback analysis, *J. Clim.*, *20*, 4497–4525, doi:10.1175/JCLI4272.1.

Lindzen, R. S., and S. Nigam (1987), On the role of sea surface temperature gradients in forcing low-level winds and convergence in the Tropics, *J. Atmos. Sci.*, *44*, 2418–2436, doi:10.1175/1520-0469(1987)044<2418:OTROSS>2.0.CO;2.

Liu, H., and G. X. Wu (1997), Impacts of land surface on climate of July and onset of summer monsoon: A study with an AGCM plus SSiB, *Adv. Atmos. Sci.*, *14*, 289–308, doi:10.1007/s00376-997-0051-8.

Liu, W. T., A. Zheng, and J. Bishop (1994), Interannual variation of the Madden-Julian oscillation during austral summer, *J. Geophys. Res.*, *99*, 12,623–12,637, doi:10.1029/94JC00604.

Meenu, S., K. Rajeev, K. Parameswaran, and C. Suresh Raju (2007), Characteristics of the double intertropical convergence zone over the tropical Indian Ocean, *J. Geophys. Res.*, *112*, D11106, doi:10.1029/2006JD007950.

Noh, Y., and H. J. Kim (1999), Simulations of temperature and turbulence structure of the oceanic boundary layer with the improved near surface process, *J. Geophys. Res.*, *104*, 15,621–15,634, doi:10.1029/1999JC900068.

Noh, Y., C. J. Jang, T. Yamagata, P. C. Chu, and C. H. Kim (2002), Simulation of more realistic upper-ocean processes from an OGCM with a new ocean mixed layer model, *J. Phys. Oceanogr.*, *32*, 1284–1307, doi:10.1175/1520-0485(2002)032<1284:SOMRUO>2.0.CO;2.

Peters, M. E., and C. S. Bretherton (2005), A simplified model of the Walker circulation with an interactive ocean mixed layer and cloud-radiative feedbacks, *J. Clim.*, *18*, 4216–4234, doi:10.1175/JCLI3534.1.

Phillips, N. A. (1973), Principles of large-scale numerical weather prediction, in *Dynamic Meteorology*, edited by P. Morel, pp. 1–96, D. Reidel, Norwell, Mass.

Ramanathan, V., and W. Collins (1991), Thermodynamic regulation of ocean warming by cirrus clouds deduced from observations of the 1987 El Niño, *Nature*, *351*, 27–32, doi:10.1038/351027a0.

Schneider, E. K. (2002), Understanding differences between the equatorial Pacific as simulated by two coupled GCMs, *J. Clim.*, *15*, 449–469, doi:10.1175/1520-0442(2002)015<0449:UDBTEP>2.0.CO;2.

Tiedtke, M. (1989), A comprehensive mass flux scheme for cumulus parameterization in large-scale models, *Mon. Weather Rev.*, *117*, 1779–1800, doi:10.1175/1520-0493(1989)117<1779:ACMFSF>2.0.CO;2.

Waliser, D. E., et al. (2003), AGCM simulations of intraseasonal variability associated with the Asian summer monsoon, *Clim. Dyn.*, *21*, 423–446, doi:10.1007/s00382-003-0337-1.

Wallace, J. M. (1992), Effect of deep convection on the regulation of tropical sea surface temperature, *Nature*, *357*, 230–231, doi:10.1038/357230a0.

Wang, B. (Ed.) (2006), *The Asian Monsoon*, 787 pp., Springer, New York.

Webster, P. J., V. O. Magana, T. N. Palmer, T. A. Tomas, N. Yanai, and T. Yasunari (1998), Monsoons: Processes, predictability, and perspectives for prediction, *J. Geophys. Res.*, *103*, 14,451–14,510.

Wu, R. G. (2002), Processes for the northeastward advance of the summer monsoon over the western north Pacific, *J. Meteorol. Soc. Jpn.*, *80*, 67–83, doi:10.2151/jmsj.80.67.

Xie, P., and P. A. Arkin (1997), Global precipitation: A 17-year monthly analysis based on gauge observations, satellite estimates, and numerical model outputs, *Bull. Am. Meteorol. Soc.*, *78*, 2539–2558, doi:10.1175/1520-0477(1997)078<2539:GPAYMA>2.0.CO;2.

Xue, Y., P. J. Sellers, J. J. Kinter, and J. Shukla (1991), A simplified biosphere model for global climate studies, *J. Clim.*, *4*, 345–364.

Yim, B. Y., S. W. Yeh, Y. Noh, B. K. Moon, and Y. G. Park (2008), Sea surface salinity variability and its relation to El Niño in a CGCM, *Asia Pac. J. Atmos. Sci.*, *44*, 173–189.

Yu, L., and R. A. Weller (2007), Objectively Analyzed air-sea heat Fluxes (OAFlux) for the global oceans, *Bull. Am. Meteorol. Soc.*, *88*, 527–539, doi:10.1175/BAMS-88-4-527.

Zeng, Q. C. (1963), Characteristic parameter and dynamical equation of atmospheric motions (in Chinese), *Acta Meteorol. Sin.*, *33*, 472–483.

Zhang, C. (2001), Double ITCZs, *J. Geophys. Res.*, *106*(D11), 11,785–11,792, doi:10.1029/2001JD900046.

Zhang, G. J., and N. A. McFarlane (1995), Sensitivity of climate simulations to the parameterization of cumulus convection in the CCC-GCM, *Atmos. Ocean*, *3*, 407–446.

Zhou, T., R. Yu, and Z. Wang (2005), *Impacts of the Ocean-Land-Atmosphere Interaction Overthe Asian Monsoon Domain on the Climate Change Over China*, vol. 4, *The Atmospheric General Circulation Model SAMIL and Its Associated Coupled Climate System Model FGOALS-s*, 288 pp., China Meteorol. Press, Beijing.

A. Duan and G. Wu, State Key Laboratory of Numerical Modelling for Atmospheric Sciences and Geophysical Fluid Dynamics, Institute of Atmospheric Physics, Chinese Academy of Sciences, PO Box 9804, Beijing 100029, China. (amduan@lasg.iap.ac.cn)

C.-H. Sui, Graduate Institute of Hydrological and Oceanic Sciences, National Central University, Jhongli 320, Taiwan.